

Shedding Light on the Weather*

Srinivasa G. Narasimhan and Shree K. Nayar
Computer Science Dept., Columbia University, New York, USA
E-mail: {srinivas, nayar}@cs.columbia.edu

Abstract

Virtually all methods in image processing and computer vision, for removing weather effects from images, assume single scattering of light by particles in the atmosphere. In reality, multiple scattering effects are significant. A common manifestation of multiple scattering is the appearance of glows around light sources in bad weather. Modeling multiple scattering is critical to understanding the complex effects of weather on images, and hence essential for improving the performance of outdoor vision systems.

We develop a new physics-based model for the multiple scattering of light rays as they travel from a source to an observer. This model is valid for various weather conditions including fog, haze, mist and rain. Our model enables us to recover from a single image the shapes and depths of sources in the scene. In addition, the weather condition and the visibility of the atmosphere can be estimated. These quantities can, in turn, be used to remove the glows of sources to obtain a clear picture of the scene. Based on these results, we demonstrate that a camera observing a distant source can serve as a “visual weather meter”. The model and techniques described in this paper can also be used to analyze scattering in other media, such as fluids and tissues. Therefore, in addition to vision in bad weather, our work has implications for medical and underwater imaging.

1 Scattering from Light Sources

Recently, there has been growing interest in the vision and image processing communities regarding image understanding in bad weather. Algorithms have been developed to recover 3D scene structure [14] and to restore clear day scene contrasts [15] and colors [14; 17] from bad weather images. Most of this work, however, assumes that the irradiance at any pixel is solely due to scattering within a small column of the atmosphere along the pixel’s line of sight. Figure 1 shows glows around light sources on a misty night. Light from the sources gets scattered multiple times and reaches the observer from different directions (figure 2). Clearly, multiple scattering of light must be modeled to better understand and exploit weather effects for improving the performance of outdoor vision systems.

*This work was supported by a DARPA HumanID Contract (N000-14-00-1-0916) and an NSF Award (IIS-99-87979).



Figure 1: Night image of light sources in mist. The glows around sources can reveal the weather condition as well as the relative depths and shapes of sources.

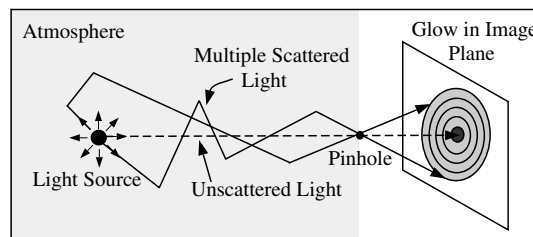


Figure 2: Multiple scattering of light from a source to a sensor results in an image with a glow around the source.

The complexity of modeling the traversal of light rays through the atmosphere is well known. One approach to solve this problem is to assume the paths of light traversal to be random and then to apply numerical Monte-Carlo techniques for ray tracing [2]. Computer graphics researchers [11; 16] have followed this approach (as well as approximations [7] like diffusion and single scattering) to render scenes in scattering media. However, millions of rays must be traced through the atmosphere to accurately model multiple scattering. Clearly, the computational complexity of this approach is too high to be suitable for most vision applications.

A different approach for modeling light scattering is the physics-based theory of radiative transfer [3; 6]. The key idea in this approach is to investigate the difference between light incident on, and exiting from, an infinitesimal volume of the medium, as shown in figure 3. Mathematically, the change in flux through a small volume is given by an integro-differential equation, called the Radiative Transfer Equation (RTE). The directional intensity at any location in the atmosphere is then obtained by solving this equation. The exact nature of the RTE depends on the locations of the radiation sources and the types and distributions of particles within the medium. Nevertheless, RTEs present a clean framework for describing multiple light scattering.

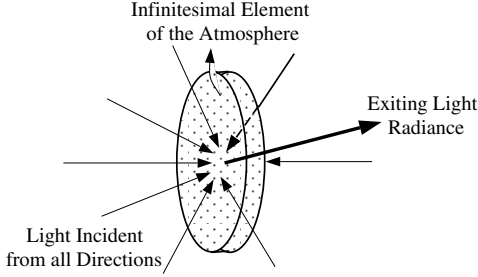


Figure 3: An infinitesimal volume of the atmosphere illuminated from all directions. The radiative transfer equation (RTE) [3] describes the relationship between scattered light radiance (in a particular direction) and the irradiance incident (from all directions) for the infinitesimal volume.

In this work, we present an analysis of how light sources appear in bad weather and what their appearances reveal about the atmosphere and the scene itself. For this, we first model multiple scattering from an *isotropic* point light source using an RTE, and solve it to obtain an analytical expression for the glow around the source. In deriving this expression, we assume that the atmosphere is homogeneous and infinite in extent. Unlike previous work on RTEs of this type [3; 8; 1; 4], our model is general and is applicable to a variety of weather conditions such as haze, fog, mist and rain.

The glow around a point source can be termed as the *atmospheric point spread function* of the source. We show that the shape of this point spread function depends on the atmospheric condition, the source intensity, and the depth of the source from the observer. Then, we describe the glows around light sources of arbitrary sizes, shapes, and intensities. It turns out that our model for the glow can be used to efficiently render realistic appearances of light sources in bad weather.

From a computer vision perspective, it is more interesting to explore how our model can be used to recover information about the scene and the atmosphere. From a single image taken at night, we compute (a) the type of weather condition, (b) the “visibility” or meteorological range, and (c) the relative depths of sources and their shapes. In addition, the glows can be removed to create a clear night view of the scene. Although we have concentrated on scattering within the atmosphere, our model is applicable to other scattering media such as fluids and tissues.

2 Scattering Properties of Weather

In this section, we discuss the scattering properties of various weather conditions. When light is incident on a particle, it gets scattered in different directions. This directional distribution of light is called the *scattering* or *phase function* of the particle. The phase function

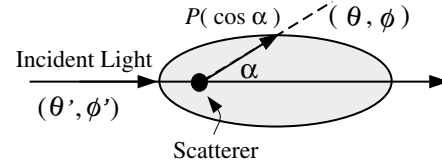


Figure 4: The phase function $P(\cos \alpha)$ is the angular scattering distribution of a particle. For most atmospheric conditions, P is symmetric about the incident light direction. The exact shape of P depends on the size of the scatterer, and hence the weather condition.

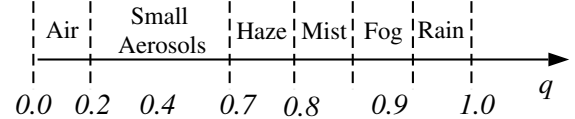


Figure 5: The approximate forward scattering parameter q of the Henyey-Greenstein phase function for various weather conditions. Note that the boundaries between the weather conditions are not clearly defined.

is denoted by $P(\theta, \phi; \theta', \phi')$ and it specifies the normalized scattered radiance in the direction (θ, ϕ) for the incident irradiance from (θ', ϕ') . For most atmospheric conditions, the phase function is known to be symmetric about the direction of incident light [3]. So, P depends only on the angle α between the directions of incident and scattered radiation (see figure 4), determined as:

$$\cos \alpha = \mu \mu' + \sqrt{(1 - \mu^2)(1 - \mu'^2)} \cos(\phi - \phi'), \quad (1)$$

where, $\mu = \cos \theta$ and $\mu' = \cos \theta'$.

The exact shape of the phase function depends on the size of the scattering particle, and hence the type of weather condition [5]. For instance, phase functions of small particles (say, air molecules) have a small peak in the direction of incidence. *Isotropic* [$P(\cos \alpha) = \text{constant}$] and *Rayleigh* [$P(\cos \alpha) = 3/4(1 + \cos^2 \alpha)$] phase functions describe the scattering from air molecules. On the other hand, phase functions of large particles (say, fog) have a strong peak in the direction of light incidence. A more general phase function that holds for particles of various sizes is the *Henyey-Greenstein phase function* [6]:

$$P(\cos \alpha) = \frac{1 - q^2}{(1 + q^2 - 2q \cos \alpha)^{3/2}}, \quad (2)$$

where, $q \in [0, 1]$ is called the *forward scattering* parameter. If $q = 0$, then the scattering is isotropic, and if $q = 1$, then all the light is scattered by the particles in the forward (incident or $\alpha = 0$) direction. Values for q between 0 and 1 can generate phase functions of most weather conditions, as shown in figure 5 [10]. We will use the Henyey-Greenstein phase function in (2) to analyze the glows observed in various weather conditions.

3 The Glow of a Point Source

In this section, we derive an analytical expression for the three-dimensional glow around an isotropic point source, that is valid for various weather conditions including fog, haze, mist, and rain. We call the glow of a point source as the *Atmospheric Point Spread Function* (APSF). The projection of the APSF onto the image plane yields the two-dimensional glow captured by a camera. Later, we describe the glows around sources of arbitrary shapes and sizes.

3.1 Atmospheric Point Spread Function

Consider an outdoor environment with a single point light source immersed in the atmosphere, as shown in figure 6. We assume that the source is isotropic i.e., the radiant intensity I_0 is constant in all directions. A pinhole camera is placed at a distance R from the point source. The multiple scattered intensities measured by the camera in different directions is the atmospheric point spread function (APSF) of the source.

The multiple scattered intensity at a radial distance R and at an angle θ with respect to the radial direction, is given by the radiative transport equation (RTE) [3]:

$$\begin{aligned} \mu \frac{\partial I}{\partial T} + \frac{1 - \mu^2}{T} \frac{\partial I}{\partial \mu} = -I(T, \mu) + \dots \\ \dots \frac{1}{4\pi} \int_0^{2\pi} \int_{-1}^{+1} P(\cos \alpha) I(T, \mu') d\mu' d\phi'. \end{aligned} \quad (3)$$

Here, $P(\cos \alpha)$ is the phase function of the particles in the atmosphere, $\mu = \cos \theta$ and $\cos \alpha$ is given by (1). $T = \sigma R$ is called the *optical thickness* of the atmosphere. The scale factor σ , called the *extinction coefficient*, denotes the fraction of flux lost due to scattering within a unit volume of the atmosphere. The “visibility”, V , is related to σ as [10]:

$$\sigma \approx \frac{3.912}{V}. \quad (4)$$

The intensity I does not depend on the azimuth angle ϕ , and hence is said to exhibit *spherical symmetry*. A closed-form solution to the above RTE, for a general phase function $P(\cos \alpha)$, has not yet been found and is conjectured to be non-existent. However, it is known that most phase functions can be approximated by a series of Legendre polynomials [3]. By expanding the Henyey-Greenstein phase function (2) in terms of Legendre polynomials, we show that a series solution to the above RTE can be obtained as:

$$I(T, \mu) = \sum_{m=0}^{\infty} (g_m(T) + g_{m+1}(T)) L_m(\mu), \quad (5)$$

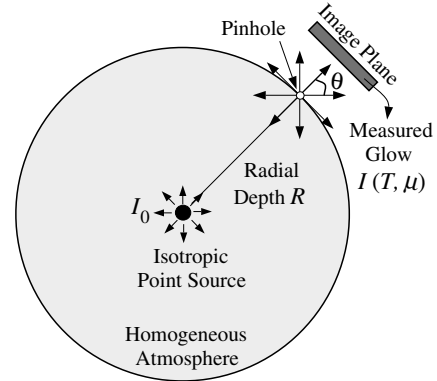


Figure 6: A homogeneous medium with spherical symmetry illuminated by an isotropic point source at the center. The scattered radiance is a function of only the radial optical thickness, $T = \sigma R$, and the inclination, $\theta = \cos^{-1} \mu$, with respect to the outward radius vector.

with $g_0 = 0$. The derivation of the above is given in the appendix. L_m is the Legendre polynomial of order m , and the m^{th} coefficient of the series g_m is given by:

$$\begin{aligned} g_m(T) &= I_0 e^{-\beta_m T - \alpha_m \log T} \\ \alpha_m &= m + 1 \\ \beta_m &= \frac{2m + 1}{m} (1 - q^{m-1}). \end{aligned} \quad (6)$$

In deriving this model, we have assumed that the atmosphere is homogeneous and infinite in extent. The function $g_m(T)$ captures the attenuation of light in bad weather, whereas the Legendre polynomial $L_m(\mu)$ explains the angular spread of the brightness observed due to multiple scattering. The glow of a particular weather condition is determined by substituting the corresponding forward scattering parameter q (figure 5) in equation (6). This model is valid for isotropic ($q = 0$) as well as anisotropic ($0 < q \leq 1$) scattering, and thus describes glows under several weather conditions.

Note that the series solution in (5) does not converge for $T \leq 1$. Fortunately, multiple scattering is very small for small optical thicknesses [9] and so the glow is not seen. We now make a few observations regarding the model and show how the shape of the glow varies with the atmospheric condition.

Angular Spread of Glow and Weather Condition:

Figure 7(a) shows cross-sections of the APSFs (normalized to $[0 - 1]$) for various weather conditions. The actual three-dimensional APSFs are obtained by rotating the cross-sections about the angle $\theta = 0$. Recall from section 2 that larger the particles, greater the forward scattering parameter q , and hence narrower or more pointed the glow. For instance, fog produces narrower glows than haze. Thus, the spread of the glow can be used for discriminating weather conditions.

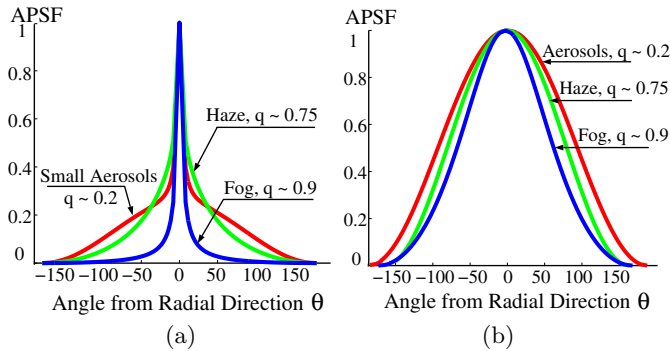


Figure 7: APSF cross-sections normalized to [0-1] for different weather conditions. (a) Haze produces a wider glow than fog but narrower than small aerosols ($T = 1.2$). (b) For highly dense atmospheres ($T = 4$), the glows are wide and different weather conditions produce similar APSFs.

Angular Spread of Glow and Weather Density: Figure 7(b) shows the APSFs for highly dense weather conditions. As the density of the particles in the atmosphere increases, the extinction coefficient σ , and hence optical thickness T , increase. For dense atmospheres, the glows are wide, and the shapes of glows for different weather conditions look similar.

Number of Coefficients (m) in the APSF: Figure 8 plots the number of coefficients m needed in the series (5) of the APSF, as a function of optical thickness T . Narrow glows (T close to 1) require a large number of coefficients in the series (5). On the other hand, wide glows require less than 10 coefficients.

3.2 Small Field of View Approximation

We derived the APSF keeping in mind a pinhole camera with a wide field of view. However, if a source and its glow are imaged from a large distance with a zoom lens (or an orthographic camera with scaling), the field of view of the source is very small (usually $< 1^\circ$). Intensities from most directions are cut-off by the lens optics. Furthermore, the magnitude of multiple scattered light is relatively small for large distances. Figure 9 illustrates this scenario. In such cases, we approximate the glow by multiple scattering (see (5)) within a small region (sphere) of the atmosphere surrounding the source multiplied by a constant attenuation factor (e^{-T}/R^2). The size of this sphere corresponds to the extent of the glow visible in the image. Note that the angle $\theta = \cos^{-1} \mu$ for which we compute multiple scattering intensity, is once again defined as the inclination to the radius vector of the sphere centered at the source.

We verified this model using images of distant sources and their glows with a high dynamic range (12-bits per pixel) Kodak digital camera. Weather data from a weather web site was obtained at the time of im-

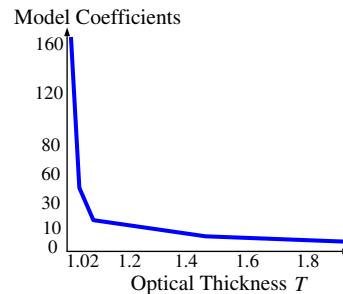


Figure 8: Number of coefficients needed in the glow model. Glows that have a sharp peak (small T) require a large number of terms in the series expansion (5), whereas less than 10 terms are needed for wide glows (large T).

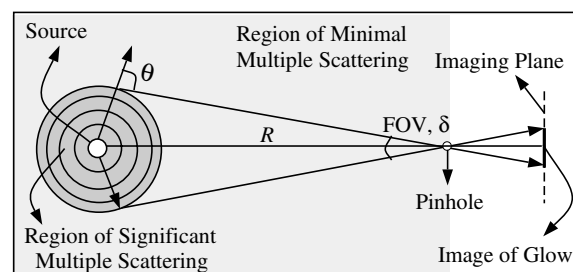


Figure 9: Multiple scattering model for large distances and small fields of view. The intensities captured by a camera is approximated by multiple scattering within a small sphere around the source multiplied by constant attenuation from the sphere boundary to the pinhole.

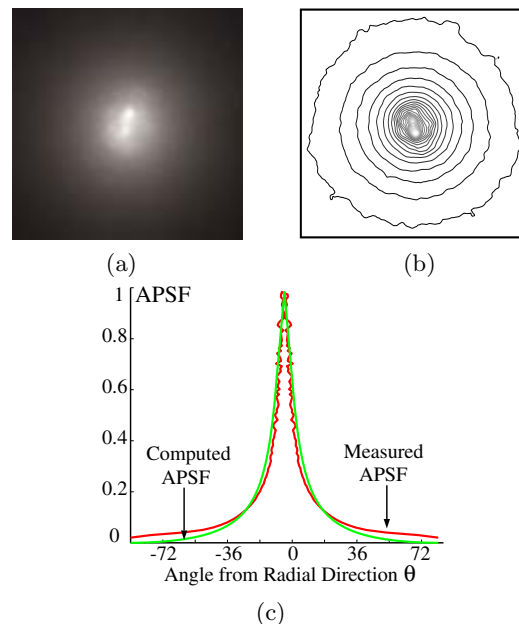


Figure 10: Verification of the glow model. (a) Image of a distant point source and its glow. (b) Iso-brightness contours of the image showing roughly concentric rings. (c) Comparison between measured and computed APSFs.

age acquisition (rain, $q \approx 0.95$, 2.25 miles visibility). The source was about 1 km away from the sensor and the field of view was 0.5° . The APSF measured from the image of the glow of one of the sources, and the APSF computed using our model are shown in figure 10. The comparison between the measured and computed APSFs shows the accuracy of our model.

4 Sources of Arbitrary Sizes and Shapes

Hitherto, we discussed the glow (APSF) of a point source seen through the atmosphere. However, sources in the real world such as street lamps, can have various shapes and sizes. We now extend the APSF to model the glows around sources of arbitrary shapes and sizes.

Sources of arbitrary shapes and sizes can be assumed to be made up of several isotropic source elements with varying radiant intensities $I_0(x, y)$ ¹. Then, by the principle of superposition of light (we assume the source elements are incoherent), the intensities due to different source elements can be added to yield the total intensity due to the light source. We assume that the entire area of the source is at roughly the same depth from an observer. Then, the light originating from each source element passes through the same atmosphere. Therefore, the image of a light source of arbitrary shape and size can be written as a convolution:

$$I = (I_0 S) * APSF. \quad (7)$$

S is a characteristic shape function that is constant over the extent of the light source (not including the glow). Since the APSF is rotationally symmetric, the above 2D convolution can be replaced by two 1D convolutions making it faster to render sources in bad weather. Figure 11 shows two sources and their simulated glows. The APSF used to convolve the source images was obtained from the real data shown in figure 10(c).

4.1 Recovering Source Shape and APSF

Consider an image of an area source in bad weather. From (7), we see that the simultaneous recovery of the APSF and the clear night view of the source ($I_0 S$) is ill-defined. However, under certain conditions, the shape of the source S can be roughly detected despite the glow around it. Note that any APSF has a peak at the center that is mainly due to the light scattered in the direction of the camera ($\theta = 0$). If this peak has much higher value than the values of neighboring directions, the actual source location in the image can be roughly detected using thresholding or high pass filtering. Figure 12 shows simulations of an actual coil shaped lamp

¹We assume that occlusions due to source elements are not significant [12] and leave a more formal treatment for future work.

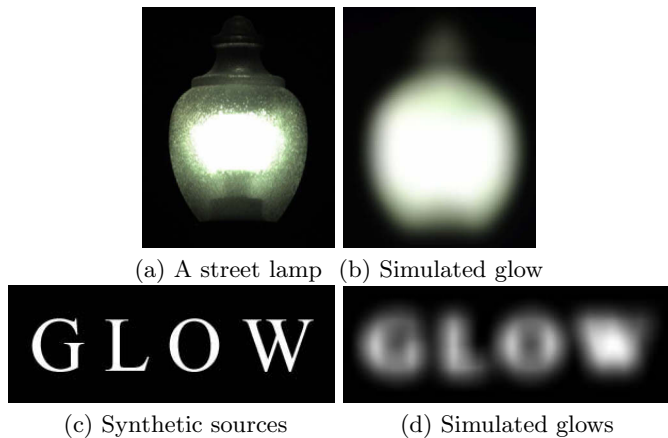


Figure 11: Rendering glows around sources in heavy mist and rain. The APSF used to render the glows was measured from an actual distant source under similar atmospheric conditions (see figure 10).

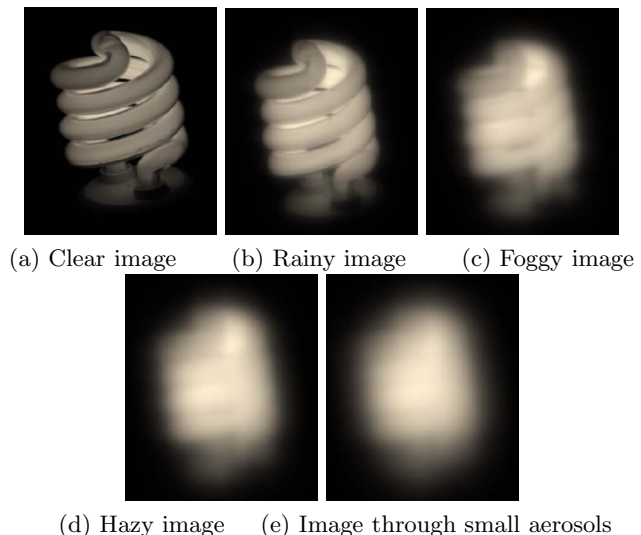


Figure 12: When can source shapes be detected? (a) Clear image of a coil shaped source. APSFs of different weather conditions with the same optical thickness, are applied to this source to obtain their glow appearances. (b) Shape can be roughly detected. (c)-(e) Hard to detect source shape.

under mild weather conditions. We conclude that it is easier to detect shapes in rain than in fog, haze or weather conditions arising due to small aerosols.

An approach for recovering source shape, and hence for removing the glow around the source, is to use the APSF computed from real data. Images of two sources with different radiant intensities, shown in figure 13(a) and (d), were captured on the same night. These sources were adjacent to one another (same depth from the camera), and hence they share the same APSF, normalized to $[0 - 1]$. We applied a simple thresholding operator to the image in figure 13(a) to obtain the shape S . We assumed that the radiant intensities I_0 of

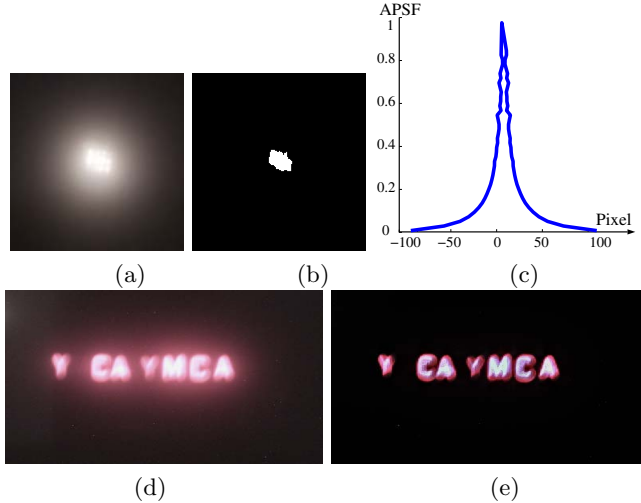


Figure 13: Shape detection, APSF computation, and glow removal. Two adjacent sources (a) and (d) of different shapes and intensities imaged under rainy and misty conditions. (b) The shape of the source in (a) is detected using simple thresholding. (c) The APSF of the source in (a) is computed using (8). (e) The APSF shown in (c) is used to remove the glow around the electronic billboard (d).

the source elements are constant across the area of the source and then recovered the normalized APSF using:

$$APSF = I * (I_0 S)^{-1}. \quad (8)$$

The normalized APSF was used to deconvolve the image of the second source (an electronic billboard) and remove the glow around the second source.

5 From APSF to Weather

In this section, we explore how our model for the APSF can be used to recover the depth of the source as well as information about the atmosphere. The APSF (5) depends on two quantities: (a) optical thickness T , which is scaled depth, and (b) forward scattering parameter q of the weather condition. The optical thickness T is related to the visibility V in the atmosphere and distance R to the source as [10]:

$$T = \sigma R \approx \frac{3.912}{V} R. \quad (9)$$

Furthermore, the value of the forward scattering parameter q can be used to find the type of weather condition (see figure 5). Given an APSF, it is therefore desirable to estimate the model parameters T and q . The APSF can either (a) be directly measured from the image (as in figure 10) when the source image lies within a pixel, or (b) be computed from the image as described in section 4.1, when the image of the source is greater than a pixel. We then use a standard optimization tool to estimate the APSF model parameters, T and q , that best fit the measured or computed APSF.

6 A Visual Weather Meter

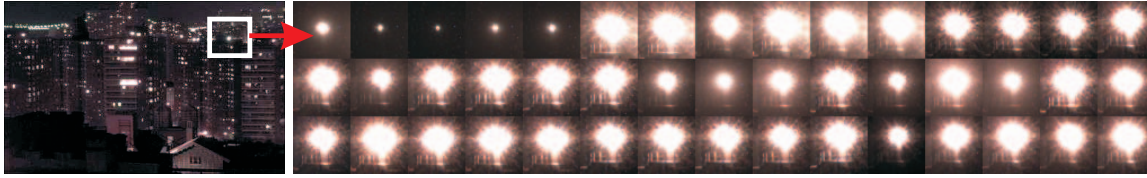
The ability to compute the type of weather and the visibility of the atmosphere from one image of a distant source turns a camera into a “Remote Visual Weather Meter”. We performed extensive experiments to test the accuracy of our techniques. We used images (figure 14(a)) of a real light source acquired under 45 different atmospheric conditions. These light source images along with ground truth weather data (type and visibility) and the actual depth of the source from the sensor, were obtained from the Columbia Weather and Illumination Database (WILD) [13].

The APSF and its parameters - optical thickness T and forward scattering parameter q were computed as described before, for each of the 45 conditions. Using the estimated T and the ground truth depth R , the visibility V was computed from (9). The estimated visibilities follow the trend of the actual visibility curve (figure 14(b)). Similarly, we used the estimates of T and the ground truth visibilities V to compute the depth R from (9). The resulting depths obtained in the 45 trials are shown in figure 14(c). The plots are normalized so that the ground truth depth is 1 unit.

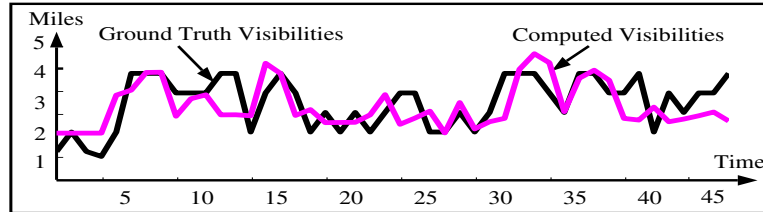
The range of estimates for q in the 45 images were between 0.75 and 1.0. These conformed to the prevalent weather conditions: haze, mist and rain (figure 14(d)). The ground truth weather data from the WILD database was collected at an observatory three miles away from the location of the source. Hence, some of the errors in the plots can be attributed to the possible incorrect ground truth data.

7 Conclusion

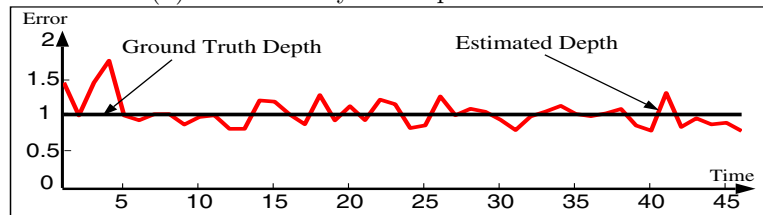
Light from sources such as street lamps and lit windows is scattered multiple times before reaching an observer. The complex multiple scattering effects give an appearance of a glow around the light source in bad weather. We presented an analytical model for the multiple scattering of light traversing through the atmosphere and showed how the shape of the glow is related to the type and visibility of the atmospheric condition, as well as the depth and shape of the light source. The model we developed can be used for real-time rendering of sources in different atmospheric conditions. The glow model was further exploited to compute scaled depth, visibility, and the type of weather condition, from a single image of a source at night. This allowed a camera to serve as a “visual weather meter”. In addition to vision in bad weather, both the model and the techniques presented here have clear implications for medical and underwater imaging.



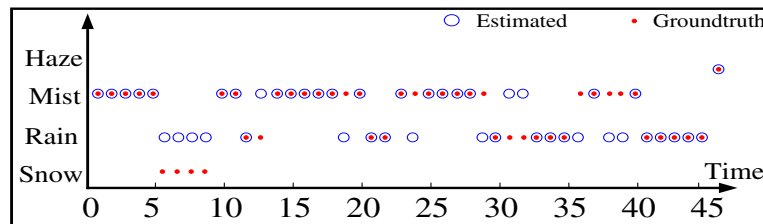
(a) A real light source viewed under 45 different atmospheric conditions.



(b) The accuracy of computed visibilities.



(b) The accuracy of computed depth.



(b) The accuracy of the computed weather condition.

Figure 14: **A Visual Weather Meter:** (a) A light source of known shape is observed under a variety of weather conditions (rain, mist, haze, snow) and visibilities (1 mile to 5 miles). Optical thickness T and forward scattering parameter q are computed from the glow observed in each image. (b) Actual ground truth depth is used to compute the visibility (see (9)). (c) To calculate depth, we used the ground truth visibilities and the computed T (see (9)). (d) Weather conditions recovered from all images. Empty circle denotes a mismatch between estimated and ground truth weather condition. The images of the sources and ground truth data were taken from the Columbia WILD database [13].

References

- [1] V. Ambartsumian. A point source of light within in a scattering medium (translated from Russian by A. Georgiev). *Bulletin of the Erevan Astronomical Observatory*, 6(3), 1945.
- [2] S. Antyufeev. *Monte Carlo Method for Solving Inverse Problems of Radiative Transfer*. Inverse and Ill-Posed Problems Series, VSP Publishers, 2000.
- [3] S. Chandrasekhar. *Radiative Transfer*. Dover Publications, Inc., 1960.
- [4] J. P. Elliott. Milne's problem with a point-source. *In Proc. Royal Soc. of London. Series A, Mathematical and Physical Sciences*, 228(1174), 1955.
- [5] Van De Hulst. *Light Scattering by small Particles*. John Wiley and Sons, 1957.
- [6] A. Ishimaru. *Wave Propagation and Scattering in Random Media*. IEEE Press, 1997.
- [7] H. W. Jensen, S. R. Marschner, M. Levoy, and P. Hanrahan. A practical model for subsurface light transport. *SIGGRAPH*, 2001.
- [8] R. E. Marshak. Note on the spherical harmonic method as applied to the milne problem for a sphere. *Physical Review*, 71(7), 1947.
- [9] E. J. McCartney. *Optics of the Atmosphere: Scattering by molecules and particles*. John Wiley and Sons, 1975.
- [10] W. E. K. Middleton. *Vision through the Atmosphere*. University of Toronto Press, 1952.
- [11] E. Nakamae, K. Kaneda, T. Okamoto, and T. Nishita. A lighting model aiming at drive simulators. *SIGGRAPH 90*.
- [12] S. G. Narasimhan and S. K. Nayar. The appearance of a light source in bad weather. *CU Tech. Report*, 2002.
- [13] S. G. Narasimhan, C. Wang, and S. K. Nayar. All the images of an outdoor scene. *In Proc. ECCV*, 2002.
- [14] S.G. Narasimhan and S.K. Nayar. Vision and the atmosphere. *IJCV*, 48(3):233–254, August 2002.
- [15] J. P. Oakley and B. L. Satherley. Improving image quality in poor visibility conditions using a physical model for degradation. *IEEE Trans. on Image Processing*, 7, Feb 1998.

[16] H. Rushmeier and K. Torrence. Zonal method for calculating light intensities in the presence of a participating medium. *SIGGRAPH 87*.

[17] Y.Y. Schechner, S.G. Narasimhan, and S.K. Nayar. Instant dehazing of images using polarization. *In Proc. CVPR*, 2001.

Solving Spherically Symmetric RTE

This appendix provides a sketch of the derivation to solve the RTE (3). More details of the derivation can be found in our technical report [12]. We begin by rewriting the RTE for a spherically symmetric atmosphere,

$$\mu \frac{\partial I}{\partial T} + \frac{1-\mu^2}{T} \frac{\partial I}{\partial \mu} = -I(T, \mu) + \frac{1}{4\pi} \int_0^{2\pi} \int_{-1}^{+1} P(\mu, \phi; \mu' \phi') I(T, \mu') d\mu' d\phi', \quad (10)$$

Integrating P over the azimuth angle, we obtain

$$P^{(0)}(\mu, \mu') = \frac{1}{2\pi} \int_0^{2\pi} P(\cos \Theta) d\phi'. \quad (11)$$

Substituting into equation 10 we get,

$$\mu \frac{\partial I}{\partial T} + \frac{1-\mu^2}{T} \frac{\partial I}{\partial \mu} = -I(T, \mu) + \frac{1}{2} \int_{-1}^{+1} P^{(0)}(\mu, \mu') I(T, \mu') d\mu', \quad (12)$$

Let $Q_m(\mu)$ be a function defined for some $m > 0$, such that

$$L_m(\mu) = \frac{d((1-\mu^2)Q_m(\mu))}{d\mu} \iff Q_m(\mu) = \frac{L'_m(\mu)}{m(m+1)}. \quad (13)$$

When there is no confusion, we drop the parameters μ and T for brevity. Multiplying 12 by Q_m and integrating with respect to μ over $[-1, +1]$, we get,

$$\int_{-1}^{+1} \mu Q_m \frac{\partial I}{\partial T} d\mu + \int_{-1}^{+1} \frac{1-\mu^2}{T} Q_m \frac{\partial I}{\partial \mu} d\mu = - \int_{-1}^{+1} Q_m I d\mu + \frac{1}{2} \int_{-1}^{+1} Q_m d\mu \int_{-1}^{+1} P^{(0)}(\mu, \mu') I(T, \mu') d\mu', \quad (14)$$

Using 13, it can be shown that [3],

$$\int_{-1}^{+1} Q_m (1-\mu^2) \left(\frac{\partial I}{\partial \mu} \right) d\mu = \int_{-1}^{+1} I(T, \mu) L_m d\mu. \quad (15)$$

Now the RTE can be rewritten as

$$\int_{-1}^{+1} \mu Q_m \frac{\partial I}{\partial T} d\mu + \frac{1}{T} \int_{-1}^{+1} L_m I d\mu = - \int_{-1}^{+1} Q_m I d\mu + \frac{1}{2} \int_{-1}^{+1} Q_m(\mu) d\mu \int_{-1}^{+1} P^{(0)}(\mu, \mu') I(T, \mu') d\mu', \quad (16)$$

Let us assume that a solution $I_m(T, \mu)$ to (16) is a product of two functions -

$$I_m(T, \mu) = g_m(T) f_m(\mu). \quad (17)$$

Substituting into 16, we get,

$$g'_m \int_{-1}^{+1} \mu Q_m f_m d\mu + \frac{g_m}{T} \int_{-1}^{+1} L_m f_m d\mu + g_m \int_{-1}^{+1} Q_m f_m d\mu - \frac{g_m}{2} \int_{-1}^{+1} Q_m d\mu \int_{-1}^{+1} P^{(0)}(\mu, \mu') f_m(\mu') d\mu' = 0. \quad (18)$$

Suppose

$$f_m(\mu) = L_{m-1} + L_m, \quad (19)$$

for some $m > 0$. The phase function P can also be expanded using Legendre polynomials:

$$P(\cos \Theta) = \sum_{k=0}^{\infty} W_k L_k(\cos \Theta). \quad (20)$$

Then, it using (1), it has been shown that [6]

$$P^{(0)}(\mu, \mu') = \sum_{k=0}^{\infty} W_k L_k(\mu) L_k(\mu'). \quad (21)$$

Similarly, we shall expand $L'_k(\mu)$ and $\mu L'_k(\mu)$ using Legendre polynomial series:

$$\begin{aligned} L'_k(\mu) &= (2k-1)L_{k-1}(\mu) + (2k-5)L_{k-3}(\mu) + \dots \\ \mu L'_k(\mu) &= kL_k(\mu) + (2k-3)L_{k-2}(\mu) + \dots \end{aligned} \quad (22)$$

We substitute equations 13, 19, 21 and 22, into equation 18 and simplify each term using the orthogonality of Legendre polynomials to get:

$$\begin{aligned} g' + \frac{g}{T} \alpha_m + g\beta_m &= 0 \\ \alpha_m = m+1 \quad \beta_m &= \left(\frac{2m+1}{m} \right) \left(1 - \frac{W_{m-1}}{2m-1} \right). \end{aligned} \quad (23)$$

For the Henyey-Greenstein phase function (2), $W_k = (2k+1)q^k$ [6]. The solution to (23) is,

$$g_m(T) = I_0 e^{-\beta_m T - \alpha_m \log T}, \quad (24)$$

where the constant of integration I_0 is the radiant intensity of the point source. Since we assume that the atmosphere is infinite in extent, the above equation automatically satisfies the boundary condition: $g_m(\infty) = 0$. Additional boundary conditions (say, camera is not outdoor) can be applied if known. For our analysis, we use the solution to the RTE given by the superposition

$$I(T, \mu) = \sum_{m=1}^{\infty} g_m(T) (L_{m-1}(\mu) + L_m(\mu)). \quad (25)$$

For convenience, we rewrite the above equation as,

$$I(T, \mu) = \sum_{m=0}^{\infty} (g_m(T) + g_{m+1}(T)) L_m(\mu), \quad g_0 = 0. \quad (26)$$